Topological *d*-wave superconductivity and nodal line-arc intersections in Weyl semimetals

Gregory A. Hamilton,[1,2] Moon Jip Park,[1,3] and Matthew J. Gilbert[2,4,5]

[1]*Department of Physics, University of Illinois at Urbana-Champaign, Urbana, Illinois 61801, USA*
[2]*Micro and Nanotechnology Laboratory, University of Illinois at Urbana-Champaign, Urbana, Illinois 61801, USA*
[3]*Department of Physics, Korea Advanced Institute of Science and Technology, Daejeon 34141, Korea*
[4]*Department of Electrical and Computer Engineering, University of Illinois at Urbana-Champaign, Urbana, Illinois 61801, USA*
[5]*Department of Electrical Engineering, Stanford University, Stanford, California 94305, USA*

(Received 30 April 2019; revised manuscript received 2 October 2019; published 24 October 2019)

Superconducting Weyl semimetals present a novel and promising system to harbor new forms of unconventional topological superconductivity. Within the context of time-reversal-symmetric Weyl semimetals with *d*-wave superconductivity, we demonstrate that the number of Majorana cones equates to the number of intersections between the *d*-wave nodal lines and the Fermi arcs. We illustrate the importance of nodal line-arc intersections by demonstrating the existence of locally stable surface Majorana cones that the winding number does not predict. The discrepancy between Majorana cones and the winding number necessitates an augmentation of the winding number formulation to account for each intersection. In addition, we show that imposing additional mirror symmetries globally protects the nodal line-arc intersections and the corresponding Majorana cones.

DOI: 10.1103/PhysRevB.100.134512

I. INTRODUCTION

Dirac and Weyl semimetals (WSMs) feature prominently in the study of topological materials alongside other semimetallic systems such as nodal line semimetals and semimetals with higher-order degeneracies [1–4]. The low-energy excitations of isolated gapless points (Weyl nodes) in the bulk Brillouin zone (BZ) of WSMs are Weyl fermions [5–7]. Weyl nodes are twofold band degeneracies that are present in systems with either broken time-reversal symmetry (TRS) or inversion symmetry (IS) [7–10]. In WSMs, open boundaries host topologically protected surface Fermi arcs connecting Weyl node projections of opposite chirality in momentum space [5]. WSMs have been experimentally observed in a wide range of materials, most notably in the transition metal monopnictide class [7,11–15].

The combination of WSMs and superconductivity is a powerful and robust platform for realizing novel topological phases of matter. In a topological superconductor (TSC), the quasiparticle spectrum has topologically protected, gapless Majorana modes that are essential to many topological quantum computing implementations [16]. Recent theoretical studies have primarily considered conventional (*s*-wave) or unconventional (*d*-wave) pairing in IS WSMs via bulk doping [17–21] or proximity effects [17,22–25]. In the case of TRS WSMs, TRS superconducting pairing between Weyl nodes of opposite momentum and equal chirality opens a bulk superconducting gap as long as the pairing potential does not vanish at the Weyl nodes [26]. In fully gapped superconductors, the sign of the pairing potential, combined with Fermi surfaces possessing nonzero chirality, define the topological invariants for classes of three-dimensional TRS TSCs [27]. Within the weak superconducting pairing limit, the relevant topological invariant is the winding number, given by

$$N_w = \frac{1}{2}\sum_s C_s \mathrm{sgn}\Delta_s. \tag{1}$$

Here C_s denotes the first Chern number on the sth disconnected Fermi surface, and Δ_s denotes the effective pairing gap on the sth Fermi surface. Equation (1) determines the number of protected gapless modes along an open boundary. Furthermore, Eq. (1) indicates sign changes in the pairing potential are an important ingredient to realize TSC, as a constant pairing potential implies, by the Nielsen-Ninomiya theorem, a trivial winding number [28]. However, unconventional nodal superconductivity, such as TRS *d*-wave superconductivity, naturally possesses sign changes in the pairing potential. Therefore, a TRS WSM with *d*-wave superconductivity is a natural candidate for TSC.

In this work, we study TSC in TRS WSMs with *d*-wave superconductivity. We demonstrate that intersections between the Fermi arcs and the nodal lines in the pairing potential naturally host Majorana cones. Interestingly, we show that additional, locally stable Majorana cones occur at the nodal line-arc intersections (NAIs) that the winding number cannot account for. Confronting this winding number limitation prompts a more careful study of the interplay between the WSM topology and the superconducting pairing potential to determine the presence of TSC. We address the limitation by recasting Eq. (1) to give an alternative definition of the winding number as a function of NAIs. Motivated by the mirror symmetries present in TRS WSMs such as TaAs and TaP [11,13–15], we consider the addition of mirror symmetries and determine the augmented topological classification that crucially depends upon the nature of NAIs.

II. THE WINDING NUMBER

We begin with a phenomenological Bogoliubov–de Gennes (BdG) Bloch Hamiltonian that describes TRS WSMs with d-wave pairing,

$$h_{\mathrm{BdG}}(\boldsymbol{k}) = \begin{pmatrix} h_0(\boldsymbol{k}) & \Delta(\boldsymbol{k}) \\ \Delta^\dagger(\boldsymbol{k}) & -h_0^*(-\boldsymbol{k}) \end{pmatrix}. \quad (2)$$

In this formulation, $h_{\mathrm{BdG}}(\boldsymbol{k})$ acts on the Nambu spinor $\Phi_{\boldsymbol{k}} = (\Psi_{\boldsymbol{k}}, \Psi^\dagger_{-\boldsymbol{k}})^T$ [17,29], and $\Delta(\boldsymbol{k})$ and $h_0(\boldsymbol{k})$ denote the d-wave pairing matrix and the TRS WSM Bloch Hamiltonian, respectively. The full Hamiltonian written in terms of Eq. (2) commutes with both the TRS and particle-hole symmetry operators. In terms of $h_{\mathrm{BdG}}(\boldsymbol{k})$, these symmetries are written as $U\mathcal{K}$, where U is a unitary operator, and $\mathcal{K}$ is complex conjugation. $U_T := is_y$, $U_C := i\tau_x$ act on $h_{\mathrm{BdG}}(\boldsymbol{k})$ as

$$\begin{aligned} U_T h^*_{\mathrm{BdG}}(-\boldsymbol{k})U_T^{-1} &= h_{\mathrm{BdG}}(\boldsymbol{k}), \\ -U_C h_{\mathrm{BdG}}(-\boldsymbol{k})U_C^{-1} &= h_{\mathrm{BdG}}(\boldsymbol{k}), \end{aligned} \quad (3)$$

where $\boldsymbol{\tau}, \boldsymbol{s}$ denote the Pauli spin vectors in the Nambu and spin spaces, respectively. Due to TRS, a Weyl node and its TRS partner have the same chirality, thereby ensuring a gapped bulk quasiparticle spectrum in the presence of d-wave superconductivity, as long as the Weyl nodes do not occur at nodal lines [26]. TRS further prohibits a complex phase in the pairing potential [21], implying that sign changes accompany nodal lines in the superconducting order parameter.

We now consider an open boundary in the $\hat{z}$ direction and assume that the superconducting pairing potential has no dependence on k_z. Figure 1 depicts a hypothetical configuration

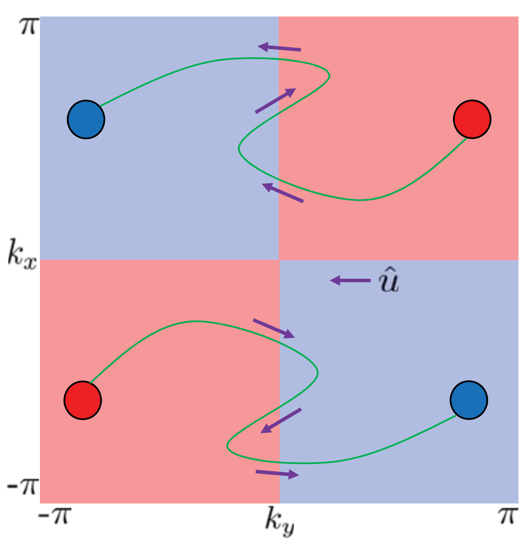

FIG. 1. Schematic of Fermi arcs (green) in a TRS WSM intersecting nodal lines in the d_{xy}-pairing potential at an open boundary. The blue (red) points depict surface Weyl node projections of negative (positive) chirality. The same coloring scheme indicates the different signed regions of the d_{xy}-pairing potential. The tangential arrows $\hat{u}_i$ depict chiral flow from the positive- to negative-chirality Weyl node projections.

of Fermi arcs connecting Weyl node projections at the open $\hat{z}$ boundary where the nodal lines of a d_{xy}-pairing potential are superimposed. By Eq. (1), the winding number is $N_w = 2$ for this configuration of Weyl nodes. In general, a nonzero N_w implies that, for any normal phase Fermi arc configuration, at least $|N_w|$ intersections between Fermi arcs and nodal lines in the pairing potential must occur, as shown in Fig. 1.

To relate the NAIs and the bulk winding number, we introduce an orientation of the Fermi arcs that starts at the positive-chirality Weyl node projection and ends at the negative-chirality Weyl node projection. The oriented NAIs allow us to recast the winding number as

$$N_w = -\sum_i \mathrm{sgn}(\nabla\Delta_i \cdot \hat{u}_i), \quad (4)$$

where i sums over all the NAIs in the BZ, $\nabla\Delta_i$ is the gradient of the pairing gap function at the intersection, and $\hat{u}_i$ is a unit vector tangent to the Fermi arc at the intersection and pointing along the orientation of the arc.

To illustrate the importance of NAIs in understanding the nature of the surface physics, we note that, by definition, $\Delta(\boldsymbol{k}) = 0$ at NAIs. At these momenta, $h_{\mathrm{BdG}}(\boldsymbol{k})$ decouples into particle and hole sectors

$$h_{\mathrm{BdG}}(\boldsymbol{k}) \cong h_0(\boldsymbol{k}) \oplus -h_0^*(-\boldsymbol{k}). \quad (5)$$

A Fourier transform in the open boundary direction $\hat{z}$ leaves $h_{\mathrm{BdG}}(\boldsymbol{k}_\parallel, z)$ block diagonal, where $\boldsymbol{k}_\parallel = (k_x, k_y)$. If $u(\boldsymbol{k}_\parallel, z)$ is a zero-energy surface eigenstate of $h_0(\boldsymbol{k}_\parallel, z)$, then $v(\boldsymbol{k}_\parallel, z) := u^*(-\boldsymbol{k}_\parallel, z)$ is a zero-energy surface eigenstate of $h_0^*(-\boldsymbol{k}_\parallel, z)$. Similarly, by TRS, $Th_0^*(-\boldsymbol{k}_\parallel, z)T^{-1} = h_0(\boldsymbol{k}_\parallel, z)$; thus, $Tu(\boldsymbol{k}_\parallel, z)T^{-1} = v(\boldsymbol{k}_\parallel, z)$, which implies $u^*(-\boldsymbol{k}_\parallel, z) = v(\boldsymbol{k}_\parallel, z)$. Therefore, the Bogoliubov transformation,

$$\gamma_{\boldsymbol{k}_\parallel, z} = u(\boldsymbol{k}_\parallel, z)\Psi_{\boldsymbol{k}_\parallel, z} + v(\boldsymbol{k}_\parallel, z)\Psi^\dagger_{-\boldsymbol{k}_\parallel, z}, \quad (6)$$

which is the eigenstate of the surface Hamiltonian, satisfies $\gamma^\dagger_{\boldsymbol{k}_\parallel, z} = \gamma_{-\boldsymbol{k}_\parallel, z}$. This is precisely the criterion for a Majorana operator under open boundary conditions [30]. The linear dispersion of both the Fermi arc and the pairing potential at the nodal line ensures Majorana surface cones occur at every NAI.

Equation (4) makes clear that the total number of NAIs and thus Majorana cones is not equivalent to the number of topological Majorana cones. Thus, additional Majorana cones beyond those required by the winding number occur as pairs in the quasiparticle spectrum. Due to chirality, these additional unprotected Majorana gap pairwise when brought together in momentum space by an adiabatic deformation of the Fermi arc configuration. Therefore, if the number of NAIs is preserved, then the accidental Majorana cones are stable in the clean limit.

III. MIRROR SYMMETRY AUGMENTATION

The inclusion of mirror symmetries such as those present in TaAs and TaP fundamentally alters the topological structure of the BdG Hamiltonian, thus changing the number of topologically protected Majorana modes at NAIs. To illustrate how the topological protection at NAIs changes under mirror symmetry, we consider the tight-binding TRS WSM

Hamiltonian [31]

$$\begin{aligned} h_0(\boldsymbol{k}) = {} & [m_z + A(3 - \cos k_0 \cos 2k_x - \cos k_y - \cos k_z]\sigma_z \\ & + B \sin k_0\{\cos 2k_x[(1-\lambda) + \lambda \cos 2k_y]\}\sigma_x \\ & + B \cos k_0 \sin 2k_x \sigma_x s_y + B \sin k_z \sigma_y \\ & + A \sin k_0 \sin 2k_x \sigma_z s_y + \frac{\lambda}{2}(\sin k_y s_x - \sin k_x s_y), \quad (7) \end{aligned}$$

where σ_i are the Pauli matrices that act on orbital space. The parameters A, B, and λ break IS that, by definition, sends $\boldsymbol{k} \to -\boldsymbol{k}$. The last term is a Rashba coupling term that alters the connectivity of the Fermi arcs when λ is changed, as described below. $h_0(\boldsymbol{k})$ also respects the mirror symmetries $M_{x/y} := is_{x/y}$. The superconducting pairing matrix takes the form

$$\Delta(\boldsymbol{k}_\parallel) := i\Delta_\alpha(\boldsymbol{k}_\parallel)\sigma_0 s_y, \quad (8)$$

where Δ_α denotes the two types of d-wave pairing gap functions, either Δ_{xy} or $\Delta_{x^2-y^2}$, given by

$$\begin{aligned} \Delta_{xy}(\boldsymbol{k}_\parallel) &= \Delta_0 \sin k_x \sin k_y, \\ \Delta_{x^2-y^2}(\boldsymbol{k}_\parallel) &= \Delta_0(\cos k_x - \cos k_y). \quad (9) \end{aligned}$$

Since the pairing potential vanishes at nodal lines for both intra- and interorbital pairing, we include only intraorbital pairing and set the magnitude to be $\Delta_0 = 1$.

In the BdG Hamiltonian, $h_{\mathrm{BdG}}(\boldsymbol{k})$ satisfies M_i symmetry if

$$M_i h_{\mathrm{BdG}}(k_i, \boldsymbol{k}) M_i^{-1} = h_{\mathrm{BdG}}(-k_i, \tilde{\boldsymbol{k}}), \quad (10)$$

where $\tilde{\boldsymbol{k}}$ denotes the momenta unaffected by M_i. For $d_{x^2-y^2}$ pairing, the mirror symmetries are given by $M_x = i\tau_z s_x$, $M_y = is_y$, while for d_{xy} pairing the mirror symmetries are written as $M_x = is_x$, $M_y = i\tau_z s_y$. The difference in the form of M_i between the two types of d-wave pairing arises from a $U(1)$-gauge choice in the hole sector of $h_{\mathrm{BdG}}(\boldsymbol{k})$ [17]. Specifically, if M_i^0 acts on $h_0(\boldsymbol{k})$, then $M_i^{\mathrm{BdG}} = M_i^0\tau_0$ or $M_i^{\mathrm{BdG}} = M_i^0\tau_z$, depending on whether or not the pairing potential changes sign under the mirror reflection.

To determine the topological classification under M_i symmetry, we utilize the minimal Dirac Hamiltonian method, briefly summarized in Appendix B, which involves analyzing the existence or nonexistence of additional symmetry-preserving extra mass terms in topological Dirac Hamiltonians [32–34]. The extra mass terms depend upon indices η_T^i, η_C^i, which, respectively, satisfy [35]

$$\begin{aligned} M_i U_T \mathcal{K} &= -\eta_T^i U_T \mathcal{K} M_i, \\ M_i U_C \mathcal{K} &= -\eta_C^i U_C \mathcal{K} M_i. \quad (11) \end{aligned}$$

There is a profound difference in the topological classification of the BdG Hamiltonian depending on the values of η_T^i, η_C^i. To illustrate the difference, we begin with $d_{x^2-y^2}$ pairing, which corresponds to $\eta_T = -1$, $\eta_C = -1$. We find that $d_{x^2-y^2}$ pairing is always topologically trivial under both M_x and M_y symmetries. We may understand the emergence of trivial topology in the presence of $d_{x^2-y^2}$ pairing by considering a bulk Weyl node situated away from any high-symmetry points in the BZ and its TRS partner of the same chirality. Upon including either M_x or M_y symmetry, both Weyl nodes now have a partner of opposite chirality, as

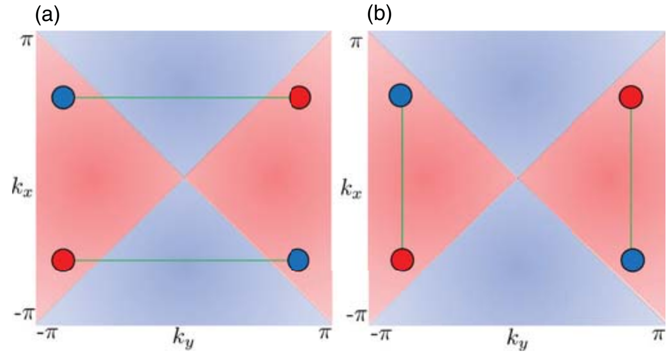

FIG. 2. (a) and (b) Allowed Fermi arc connectivities under a fixed configuration of Weyl nodes on an open boundary with the $d_{x^2-y^2}$-pairing potential superimposed on the plot. Here the winding number is trivial, as the minimal number of NAIs is zero in (b).

depicted in Fig. 2(a). Neighboring nodes of opposite chirality always occur in regions of the same sign of the pairing potential. Equation (4) then implies that the contribution of each pair of neighboring nodes to the winding number vanishes. Furthermore, for $d_{x^2-y^2}$ pairing there always exists a Fermi arc configuration wherein neighboring Weyl nodes in the same sign of pairing potential may be connected, thus implying the winding number vanishes, as shown in Fig. 2(b).

In contrast to $d_{x^2-y^2}$ pairing, d_{xy} pairing, corresponding to $\eta_T = -1$, $\eta_C = 1$, supports a $\mathbb{Z} \oplus \mathbb{Z}$ classification [32]. The first $\mathbb{Z}$ index corresponds to the winding number as given in Eq. (4), while the latter index corresponds to the mirror strong index $N_{M_i\mathbb{Z}}$. While the topological classification is extended under d_{xy} pairing to include two invariants, the number of protected Majorana modes is given by $\max(|N_{M_i\mathbb{Z}}|, |N_w|)$ [32]. Assuming a generic $h_0(\boldsymbol{k})$ respects M_y symmetry, we block diagonalize $h_{\mathrm{BdG}}(\boldsymbol{k})$ into $h_{\mathrm{BdG},+i}(\boldsymbol{k}) \oplus h_{\mathrm{BdG},-i}(\boldsymbol{k})$, where $\pm i$ are the eigenvalues of M_y. The mirror strong index is then given by [32]

$$N_{M_y\mathbb{Z}} = \mathrm{sgn}\big(M\mathbb{Z}_0^{\mathrm{BdG}} - M\mathbb{Z}_\pi^{\mathrm{BdG}}\big)\big(\big|M\mathbb{Z}_0^{\mathrm{BdG}}\big| - \big|M\mathbb{Z}_\pi^{\mathrm{BdG}}\big|\big). \quad (12)$$

Here the mirror Chern number $M\mathbb{Z}_i^{\mathrm{BdG}}$ is defined as

$$M\mathbb{Z}_i^{\mathrm{BdG}} = \tfrac{1}{2}\big(C_i^{+,\mathrm{BdG}} - C_i^{-,\mathrm{BdG}}\big), \quad (13)$$

where $C_i^{+,\mathrm{BdG}}$ denotes the Chern number for $h_{\mathrm{BdG},+}$ on the surface $k_y = i$ in the bulk Brillouin zone [36].

Turning to the tight-binding model given in Eq. (7), we choose the parameters A, B, k_0, and m_z such that eight zero-energy Weyl nodes are located in the BZ, as shown in Fig. 3(a). In Fig. 3(a), we show the Zak phase corresponding to $h_0(\boldsymbol{k})$ ($\lambda = 0$) along the $\hat{z}$ boundary, defined to be $\gamma^Z(\boldsymbol{k}_\parallel) = \oint dk_z A(\boldsymbol{k})$, where $A(\boldsymbol{k})$ is the Berry connection. The regions where the Zak phase equals π denote the locations of the four Fermi arcs, while the vorticity at the Weyl node projections indicates the sign of the chirality of the bulk Weyl node [37,38]. Including d_{xy} pairing and using Eq. (4), we find $N_w = 0$, while, in contrast, $|N_{M_y\mathbb{Z}}| = 4$. We describe the details of this calculation in Appendix A. The nonzero value of the mirror strong index is evident from the geometrical

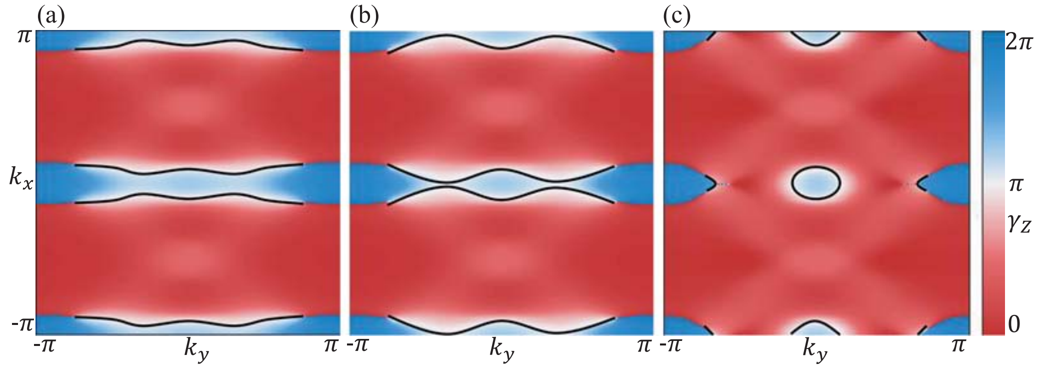

FIG. 3. The changing of the Fermi arc connectivity (black lines) in the presence of M_y symmetry. (a) The initial Fermi arc configuration ($\lambda = 0$) is shifted in (b) a mirror-symmetric manner ($\lambda = 0.1$), such that (c) the mirror Chern number forces a dangling Dirac cone to appear once the Weyl node connectivity is changed ($\lambda = 0.5$). Here we have chosen $m_z = A/(-2 + \sqrt{2}),\ k_0 = \pi/4,\ A = B = 2$.

configuration of the Fermi arcs. Since the pairing potential vanishes along the mirror plane, the mirror strong index is simplified to $|N_{M_y\mathbb{Z}}| = |M\mathbb{Z}_0|$, where $M\mathbb{Z}_0$ denotes the mirror Chern number of $h_0(\boldsymbol{k})$. As M_y symmetry conserves the Chern number in each mirror sector, Fermi arcs with opposite chirality cannot hybridize to produce a gap at $k_y = 0$. Therefore, the number of zero modes intersecting $k_y = 0$ must be preserved. Since there are four Fermi arcs crossing $k_y = 0$ [two Fermi arcs per mirror sector, as shown in Fig. 3(a)], the mirror strong index is $|N_{M\mathbb{Z}}| = 4$. Correspondingly, the four locations where the Fermi arcs cross $k_y = 0$ exhibit Majorana modes.

We further elucidate the relation between NAIs and $N_{M_y\mathbb{Z}}$ by considering mirror-symmetric deformations of the Fermi arcs that change the connectivity of the Weyl nodes, as shown in Fig. 3. Noting that the mirror planes and nodal lines coincide, the particle and hole sectors decouple, and we may restrict our analysis to the normal-phase Hamiltonian. Starting from Fig. 3(a), we increase λ while preserving M_y symmetry, thereby changing the Fermi arc configuration to that shown in Fig. 3(b) ($\lambda = 0.1$) and, finally, arriving at Fig. 3(c) ($\lambda = 0.5$). Figure 3(c) shows the final altered Fermi arc configuration after reconnecting the Weyl nodes where, despite changing the Weyl node connectivity, the number of zero modes crossing $k_y = 0$ is conserved by the creation of a disconnected Dirac cone [39]. These dangling Dirac cones ensure that the $\mathbb{Z}$ mirror Chern number remains unchanged in the normal phase. The coincidence of nodal lines and mirror planes in d_{xy} pairing ensures the topological protection from the mirror symmetry carries through from the normal phase to the superconducting phase. Moreover, in the superconducting phase, after the deformation four surface Majorana cones appear at the NAIs along $k_x = 0$. Thus, the mirror symmetry ensures that the number of NAIs is preserved even when the Weyl node connectivity is changed.

IV. CONCLUSION

In conclusion, we considered a TRS WSM with d-wave superconductivity and analyzed the resulting topological classification and gapless surface modes. We demonstrated, both analytically and numerically, the existence of locally stable Majorana cones at NAIs that the DIII winding number does not predict. Consequently, we provided an augmentation of the winding number formalism that specifies both the number and location of all Majorana cones that occur along an open boundary in the $\hat{z}$ direction. Given the mirror symmetries inherent in many experimentally observed TRS WSMs, such as TaAs, TaP, and NbAs, we further analyzed how the topological classification changes when we incorporate the mirror symmetries of both the TRS WSM and the d-wave pairing potential. We found that the mirror symmetries of the two d-wave pairing potentials considered, d_{xy} and $d_{x^2-y^2}$ pairing, give rise to drastically different topological classifications. The mirror symmetry under d_{xy} pairing protects surface Majorana cones, even when the Fermi arc connectivity is changed in a mirror-symmetric manner, while the mirror symmetry of $d_{x^2-y^2}$ pairing renders the system topologically trivial. Our results further extend predictions of topological superconductivity in TRS WSMs and highlight the crucial roles unconventional superconductivity, crystalline symmetries, and Fermi arcs play in understanding these exotic systems.

ACKNOWLEDGMENTS

G.A.H., M.J.P., and M.J.G. acknowledge financial support from the National Science Foundation (NSF) under Grant No. DMR-1720633. M.J.P. is supported by the BK21 plus program, KAIST, and the National Research Foundation Grant No. NRF2017R1A2B4008097. M.J.G. acknowledges support from the NSF under CAREER Award No. ECCS-1351871 and the Office of Naval Research (ONR) under Grant No. N00014-17-1-3012. G.A.H. acknowledges fruitful conversations with Y. Kim, M. R. Hirsbrunner, T. M. Philip, and B. Basa.

APPENDIX A: NUMERICAL MIRROR CHERN NUMBER CALCULATION

In this Appendix, we review a numerical approach for finding the Chern number for a mirror sector. In doing so, we closely follow the notation given in [40].

We begin with a generic n-band Bloch Hamiltonian, where we label $|n(k)\rangle$ as the (normalized) nth band wave function. We define a "link" variable [40] as

$$U_\mu(\boldsymbol{k}_l) = \langle n(\boldsymbol{k}_l)|n(\boldsymbol{k}_l + \hat{\mu})\rangle / \mathcal{N}_\mu(\boldsymbol{k}_l), \quad \text{(A1)}$$

where $\hat{\mu}$ is a lattice unit vector and $\boldsymbol{k}_l$ denotes a momentum in the (discretized) lattice. Here $\mathcal{N}_\mu(\boldsymbol{k}_l) = |\langle n(\boldsymbol{k}_l)|n(\boldsymbol{k}_l + \hat{\mu})\rangle|$. Then the Chern number (explicitly summing over occupied bands) is given by

$$C_1 = \frac{1}{2\pi i}\sum_{n\in occ}\sum_l F^n_{ij}(\boldsymbol{k}_l), \quad \text{(A2)}$$

where the nth band field strength $F^n_{ij}(\boldsymbol{k}_l)$ is given by

$$F_{ij}(\boldsymbol{k}_l) = \ln U_i(\boldsymbol{k}_l)U_j(\boldsymbol{k}_l + \hat{i})U_i(\boldsymbol{k}_l + \hat{j})^{-1}U_j(\boldsymbol{k}_l)^{-1}. \quad \text{(A3)}$$

Here $\hat{i}, \hat{j}$ label unit lattice vectors, and $F_{ij}(\boldsymbol{k}_l)$ is defined within the principal branch of the logarithm [40]. In the case of degeneracies in the occupied bands, the non-Abelian connection must be used, and the link variable is replaced with

$$U_\mu(\boldsymbol{k}_l) = \det[\langle\psi(\boldsymbol{k}_l)|\psi(\boldsymbol{k}_l + \hat{\mu})\rangle]/\mathcal{N}_\mu(\boldsymbol{k}_l). \quad \text{(A4)}$$

Here as before $\mathcal{N}_\mu(\boldsymbol{k}_l) = |\det\langle\psi(\boldsymbol{k}_l)|\psi(\boldsymbol{k}_l + \hat{\mu})\rangle|$, and $\psi(\boldsymbol{k}_l)$ denotes the multiplet $(|n_1\rangle, \ldots, |n_m\rangle)$, where m is the largest degeneracy in the occupied bands.

If we have a mirror symmetry M_i for a Bloch Hamiltonian $h(\boldsymbol{k})$ that satisfies $M_i h(\boldsymbol{k}) M_i^{-1} = h(-k_i, \tilde{\boldsymbol{k}})$, where $\tilde{\boldsymbol{k}}$ denotes the momenta unchanged by M_i, then, in the plane $k_i = 0$, h commutes with M_i. h is then block diagonal in the two M_i sectors (labeled by $\pm i$); that is, $h = h^+ \oplus h^-$. With this definition, a Chern number $C^{+/-}$ may be computed for each sector. Furthermore, a mirror Chern number defined for the plane is given by [36]

$$n_{M_i} = (C^+ - C^-)/2. \quad \text{(A5)}$$

Using n_{M_i} gives the number of gapless modes along the mirror plane boundary, as seen in the main text.

APPENDIX B: MINIMAL DIRAC HAMILTONIAN METHOD

Here we give a brief overview of the minimal Dirac Hamiltonian method used to determine the topological classification under the mirror symmetry [32]. Note that we keep the mirror symmetry representation such that the eigenvalues are $\pm i$, in contrast to [32].

We write a Hamiltonian in d spatial dimensions as

$$H = m\gamma_0 + \sum_{i=1}^{d} k_i\gamma_i. \quad \text{(B1)}$$

Here m is constant, and we have the commutation and anticommutation relations

$$\begin{aligned} &\{\gamma_i, \gamma_j\} = 2\delta_{ij}\mathbb{I},\ i = 0, 1, \ldots, d, \\ &[\gamma_0, T] = 0, \quad \{\gamma_{i\neq 0}, T\} = 0, \\ &\{\gamma_0, C\} = 0, \quad [\gamma_{i\neq 0}, C] = 0, \end{aligned} \quad \text{(B2)}$$

where T, C denote time-reversal symmetry and particle-hole symmetry, respectively. If it is possible to write an extra mass term to be added into the Hamiltonian such that the new mass term anticommutes with γ_0, respects the given symmetries, and opens a gap in the spectrum of the system such that varying m in the mass term $m\gamma_0$ keeps the system in the same topological phase, then we denote this term as a symmetry-preserving extra mass term (SPEMT). If no such SPEMT term exists, then the system possesses either $\mathbb{Z}_2$ or $\mathbb{Z}$ topology. To differentiate between $\mathbb{Z}_2$ and $\mathbb{Z}$, we consider an enlarged Hamiltonian,

$$H' = \sum_i k_{n_i}\gamma_{n_i}\otimes\sigma_z + \sum_{\text{remain}} k_{n_j}\gamma_{n_j}\otimes\mathbb{I}, \quad \text{(B3)}$$

where $n_i \in (0, 1, \ldots, d)$. The second summation is over the γ matrices not included in the first summation. If a SPEMT can be added to this larger minimal Dirac Hamiltonian, then the topological classification is $\mathbb{Z}_2$.

To find the topological classification under mirror symmetry, we construct an operator $\gamma_1 R$ satisfying

$$\{\gamma_1 R, H\} = 0. \quad \text{(B4)}$$

The above operator may be added either as an extra mass term or an extra kinetic term, depending on the indices η_T, η_C stated in the main text. The addition of this operator as an extra kinetic term increases the effective dimension of the Hamiltonian, while the addition of $\gamma_1 R$ as an extra mass term decreases the effective dimension of the Hamiltonian. The topological invariants for these higher- (lower-) dimensional Hamiltonians without reflection symmetry are in one-to-one correspondence with the topological invariants of the Hamiltonian with the reflection symmetry.

[1] X.-Q. Sun, B. Lian, and S.-C. Zhang, Phys. Rev. Lett. **119**, 147001 (2017).

[2] R. Bi, Z. Yan, L. Lu, and Z. Wang, Phys. Rev. B **96**, 201305(R) (2017).

[3] C. Fang, H. Weng, X. Dai, and Z. Fang, Chin. Phys. B **25**, 117106 (2016).

[4] B. Bradlyn, J. Cano, Z. Wang, M. G. Vergniory, C. Felser, R. J. Cava, and B. A. Bernevig, Science **353**, aaf5037 (2016).

[5] N. P. Armitage, E. J. Mele, and A. Vishwanath, Rev. Mod. Phys. **90**, 015001 (2018).

[6] B. Yan and C. Felser, Annu. Rev. Condens. Matter Phys. **8**, 337 (2017).

[7] H. Weng, C. Fang, Z. Fang, B. A. Bernevig, and X. Dai, Phys. Rev. X **5**, 011029 (2015).

[8] A. A. Burkov and L. Balents, Phys. Rev. Lett. **107**, 127205 (2011).

[9] S. Murakami, New J. Phys. **9**, 356 (2007).

[10] A. Go, W. Witczak-Krempa, G. S. Jeon, K. Park, and Y. B. Kim, Phys. Rev. Lett. **109**, 066401 (2012).

[11] S.-M. Huang, S.-Y. Xu, I. Belopolski, C.-C. Lee, G. Chang, B. Wang, N. Alidoust, G. Bian, M. Neupane, C. Zhang, S. Jia, A. Bansil, H. Lin, and M. Z. Hasan, Nat. Commun. **6**, 7373 (2015).

[12] C.-K. Chiu, J. C. Y. Teo, A. P. Schnyder, and S. Ryu, Rev. Mod. Phys. **88**, 035005 (2016).

[13] B. Q. Lv, H. M. Weng, B. B. Fu, X. P. Wang, H. Miao, J. Ma, P. Richard, X. C. Huang, L. X. Zhao, G. F. Chen, Z. Fang, X. Dai, T. Qian, and H. Ding, Phys. Rev. X **5**, 031013 (2015).

[14] Z. K. Liu, L. X. Yang, Y. Sun, T. Zhang, H. Peng, H. F. Yang, C. Chen, Y. Zhang, Y. F. Guo, D. Prabhakaran, M. Schmidt, Z. Hussain, S.-K. Mo, C. Felser, B. Yan, and Y. L. Chen, Nat. Mater. **15**, 27 (2015).

[15] S.-Y. Xu, N. Alidoust, I. Belopolski, Z. Yuan, G. Bian, T.-R. Chang, H. Zheng, V. N. Strocov, D. S. Sanchez, G. Chang, C. Zhang, D. Mou, Y. Wu, L. Huang, C.-C. Lee, S.-M. Huang, B. Wang, A. Bansil, H.-T. Jeng, T. Neupert *et al.*, Nat. Phys. **11**, 748 (2015).

[16] C. Nayak, S. H. Simon, A. Stern, M. Freedman, and S. Das Sarma, Rev. Mod. Phys. **80**, 1083 (2008).

[17] M. Sato and Y. Ando, Rep. Prog. Phys. **80**, 076501 (2017).

[18] B. Lu, K. Yada, M. Sato, and Y. Tanaka, Phys. Rev. Lett. **114**, 096804 (2015).

[19] Y. Li and F. D. M. Haldane, Phys. Rev. Lett. **120**, 067003 (2018).

[20] G. Bednik, A. A. Zyuzin, and A. A. Burkov, Phys. Rev. B **92**, 035153 (2015).

[21] P. Hosur, X. Dai, Z. Fang, and X.-L. Qi, Phys. Rev. B **90**, 045130 (2014).

[22] H. Wang, H. Wang, Y. Chen, J. Luo, Z. Yuan, J. Liu, Y. Wang, S. Jia, X.-J. Liu, J. Wei, and J. Wang, Sci. Bull. **62**, 425 (2017).

[23] U. Khanna, A. Kundu, S. Pradhan, and S. Rao, Phys. Rev. B **90**, 195430 (2014).

[24] Y. Kim, M. J. Park, and M. J. Gilbert, Phys. Rev. B **93**, 214511 (2016).

[25] A. Chen and M. Franz, Phys. Rev. B **93**, 201105(R) (2016).

[26] T. Meng and L. Balents, Phys. Rev. B **86**, 054504 (2012).

[27] X.-L. Qi, T. L. Hughes, and S.-C. Zhang, Phys. Rev. B **81**, 134508 (2010).

[28] H. Nielsen and M. Ninomiya, Phys. Lett. B **105**, 219 (1981).

[29] N. N. Bogoljubov, Nuovo Cimento **7**, 794 (1958).

[30] K. Björnson and A. M. Black-Schaffer, Phys. Rev. B **91**, 214514 (2015).

[31] This Hamiltonian is inspired by Ref. [22].

[32] C.-K. Chiu, H. Yao, and S. Ryu, Phys. Rev. B **88**, 075142 (2013).

[33] K. Shiozaki and M. Sato, Phys. Rev. B **90**, 165114 (2014).

[34] A. P. Schnyder, S. Ryu, A. Furusaki, and A. W. W. Ludwig, Phys. Rev. B **78**, 195125 (2008).

[35] In contrast to the convention in Ref. [32], we do not force M_i to be Hermitian.

[36] J. C. Y. Teo, L. Fu, and C. L. Kane, Phys. Rev. B **78**, 045426 (2008).

[37] J. Zak, Phys. Rev. Lett. **62**, 2747 (1989).

[38] K. W. Kim, W.-R. Lee, Y. B. Kim, and K. Park, Nat. Commun. **7**, 13489 (2016).

[39] The dangling Dirac cones are distinct from the dangling Dirac cones related to the $\mathbb{Z}_2$ weak indices derived from TRS in [41], as the number of Dirac cones present in this case are protected by a $\mathbb{Z}$ rather than a $\mathbb{Z}_2$ invariant.

[40] T. Fukui, Y. Hatsugai, and H. Suzuki, J. Phys. Soc. Jpn. **74**, 1674 (2005).

[41] A. Lau, K. Koepernik, J. Van Den Brink, and C. Ortix, Phys. Rev. Lett. **119**, 076801 (2017).